CEM CODE VALIDATION USING INFRARED THERMOGRAMS

John Norgard
Electromagnetics Laboratory
Department of Electrical & Computer Engineering
College of Engineering & Applied Science
University of Colorado
P.O. Box 7150
Colorado Springs 80933-7150
USA

Keywords: Infrared, Thermograms, Electromagnetic, Microwave, Metrology, Correlation, Code Validation, Radiation, Scattering, Waveguide/Cavity Modes

Abstract

In this article, an infrared (IR) measurement technique is presented that has been developed to measure electromagnetic (EM) fields. This technique uses a minimally perturbing, thin, planar IR detection screen to produce a thermal image (e.g., an IR thermogram) of the intensity of the EM energy over the two-dimensional region of the screen. Several examples are presented using this thermal technique to measured EM fields. These examples include:

i)

i) radiation from microwave sources
ii) scattering from conducting bodies
iii) coupling through apertures in shielded enclosures.

These examples illustrate the use of this thermal technique to correlate theoretical data with experimental observations. This technique has also been used to experimentally validate complicated numerical codes that predict electric field distributions in areas where conventional hard-wired probes would significantly perturb the fields being measured, for example inside waveguides and cavities (E-Fields) and near apertures. Surface current distributions (H-Fields) on metallic surfaces also can be measured with this technique.

INTRODUCTION

A non-destructive, minimally perturbing infrared (IR) measurement technique has been developed to observe electromagnetic (EM) fields. Metallic surface currents and charges also can be measured with this technique.

This IR measurement technique produces a two-dimensional IR thermogram of the electric or magnetic field being measured, i.e. a two-dimensional gray-scale image of the measured temperature profile in the screen. After calibration, the temperature data can be presented as a two-dimensional isothermal contour map or a three-dimensional relief map of the intensity of the EM field incident on the screen.

The IR measurement technique has been applied to determine:

a. The radiated fields from microwave antennas and high-power microwave (HPM) sources, e.g. near-field intensities and far-field antenna patterns of horn antennas [1];
b. Diffraction patterns of EM fields scattered from complicated metallic objects [2,3];
c. Intensities of EM fields coupled through apertures in shielded enclosures [4]; and
d. Modal distributions of EM fields excited inside cavities [5,6].

Electric and magnetic fields can be measured separately. Examples are presented of the thermal images of electric field distributions

- radiated from microwave horn antennas
- coupled through apertures
- induced inside waveguide cavities (internal cylindrical cavity modes).

Examples of magnetic field distributions near conductive surfaces and induced surface currents on metallic surfaces have also been taken.

The advantages and disadvantages of this new IR measurement technique are also discussed.

IR MEASUREMENT TECHNIQUE

The IR measurement technique is based on the Joule heating that occurs in a lossy material as an EM wave passes through the material. A thin, planar sheet of a lossy carbon loaded paper or a carbon loaded polyimide film are used to map electric fields; a thin, planar sheet of a lossy ferrite loaded epoxy is used to map magnetic fields. In either situation, the absorbed heat energy is converted into conducted and convected heat energy and into re-radiated EM energy. The radiated EM energy is concentrated in the IR band. This "black body" energy is detected with an IR (Scanning) Array or with an IR (Staring) Focal Plane Array (FPA).

IR Experimental Setup

This technique involves placing a lossy, non-perturbing IR detection screen near the source of the EM energy in the plane (or planes) over which the field is to be measured.

Electromagnetic Parameters. The detector screen is made from a thin sheet of linear, homogenous, and isotropic lossy material. From the complex form of Poynting's Theorem for a linear, homogeneous, and isotropic material, the absorbed power P_{abs} within the given volume V of the lossy material is a function of the electric (E) and magnetic (H) field intensities inside the screen and is given by

$$P_{abs} = \int_v (\sigma E^2 + \omega \varepsilon'' E^2 + \omega \mu'' H^2) dv \qquad (1)$$

where σ is the conductivity of the detector screen, ε'' is the imaginary component of the permittivity (dielectric constant) of the detector screen, μ'' is the imaginary component of the permeability of the detector screen, and ω is the radian frequency of the incident field. The volume integral is over the illuminated portion of the detector screen. The spectral characteristics of the complex constitutive parameters $(\mu, \varepsilon, \sigma)$ must be known (or measured) over the entire frequency bandwidth of interest in the measurements.

Electric and magnetic field detector screens have been designed and fabricated to be sensitive to only one component of the magnitude of the electric or magnetic fields, as discussed below.

The incident EM energy is absorbed by the lossy material and is converted into thermal heat energy, which causes the temperature of the detector material to rise above the ambient temperature of the surrounding background environment by an amount that is proportional to the local electric and/or magnetic field intensity (energy) at each point (pixel) in the screen material. In regions where the field is strong, the absorbed energy is large and the resulting pixel temperatures are high; in regions where the field is weak, the absorbed energy is small and the resulting pixel temperatures are low. The resulting two-dimensional temperature distribution over the surface of the screen is detected, digitized, and stored in the memory of the IR camera.

The temperature distribution on the surface of the screen without any EM energy incident on the screen is also stored in the memory of the IR camera as an ambient background reference temperature distribution. The difference in the temperature at each pixel location between the illuminated and the non-illuminated screens is a result of only the effects of the electric or magnetic field incident on the screen at each pixel location. These EM effects can be visualized by presenting the differenced two-dimensional temperature profile as a false color image, where cool colors (for example shades of blue) represent weak areas of EM energy and hot colors (for example shades of red) represent strong areas of EM energy. The resulting two-dimensional false color image is called an IR thermogram, i.e., an iso-temperature contour map, and is a representation of the electric and/or magnetic electric field distribution passing through the screen material.

Thermal Parameters. For a planar sheet of detector material supported by a block of non-conducting material, i.e., a styrofoam block, the thermal heat transfer problem reduces to considering only the radiative and convective heat losses from the front surface of the detector material.

The convective heat loss h_{conv} is approximated by

$$h_{conv} = h_o (T - T_{amb})^{1.25} \quad [W/m^2] \qquad (2)$$

where h_o varies between 1.4 and 1.6, depending on the detector screen material.

The radiative heat loss h_{rad} is approximated by

$$h_{rad} = \varepsilon_{IR} \sigma_{IR} (T^4 - T_{amb}^4) \quad [W/m^2] \qquad (3)$$

where ε_{IR} is the detector surface emissivity (not to be confused with the electric dielectric constant ε), σ_{IR} is the Stefan-Boltzman constant in W/m^2K^4 (not to be confused with the electric conductivity σ).

The conductive heat loss h_{cond} is negligibly small, and is approximated by

$$h_{cond} \cong 0 \quad [W/m^2] \qquad (4)$$

In the above equations, all temperatures are in degrees Kelvin.

Thermal Equilibrium. The heat transfer problem in the detector material involves solving a non-linear, second-order differential equation in both space and time, while considering radiative and convective (negligible conduction) heat losses from the surface of the material, conductive heat transfer inside the material, and EM power absorption in the material as a function of distance into the material. For the case of the thin detector screens considered here, the transverse temperature distribution is initially considered to be constant in the axial direction normal to the surface of the material, so that the conductive term normal to the surface of the screen can also be ignored and the power absorbed can be considered independent of the direction normal to the surface of the screen. Also, the time dependence of the absorbed heat energy can be ignored for the steady-state solution that follows.

Relating the convective, conductive, and radiative heat losses in equations (2) and (4) to the absorbed power in equation (1), results in the following equation at thermal equilibrium:

$$P_{abs} \cong h_{rad} + h_{conv} + \underbrace{h_{cond}}_{\cong 0} \qquad (5)$$

For a properly optimized detector screen, thermal equilibrium is achieved in just a few seconds.

This non-linear thermal/electrical equation can be solved for the temperature T of the detector material, as a function of the incident electric and or magnetic field, using approximate techniques to solve Maxwell's Equations (Snell's Laws and Fresnel's Laws) and the Heat Equation for a plane wave incident on a four layered (air/screen/insulator/air) planar film of lossy material in thermal equilibrium. This solution can then be inverted numerically for the incident electric or magnetic field intensity as a function of the screen temperature. The inverted result is then fitted with a high-order polynomial to yield a calibration curve (formula) for the detector screen material.

The theoretical solution was verified experimentally at NIST/Boulder. A calibrated standard gain horn was used to irradiate the screen with a precisely known near-field intensity (at the surface of the screen). The intensity of the field was increased, from initial detection to final saturation of the difference temperature. At each intensity, the IR camera was used to measure the resulting surface temperature (color) of the screen. A "color" table of temperature verse incident field strength was developed, which agreed well with the theoretically derived results discuss above. A simple table-look-up scheme can then be used to convert temperature into field intensity. Approximately 30 dB of dynamic range is available in the thermal technique when a scanning array is used as the IR detector and approximately 40 dB of dynamic range is available when a FPA is used.

Approximate Solution

Equation (5) is a highly non-linear equation for large temperature variations above ambient, due to the thermal processes of convection and radiation. However, for small temperature variations of only a few tenths of a degree above ambient, equation (5) can be linearized for small incremental temperature changes $\Delta T = T - T_{amb}$ above the ambient temperature T_{amb}.

This condition of small temperature variations above ambient is a desirable operational constraint, because this is also the requirement for small absorption of the

EM energy passing through the screen, which equates to small perturbations of the incident field to perform the measurement. For this minimally perturbing measurement case, an almost direct linear correlation exists between the incremental surface temperature ΔT and the electric or magnetic field intensity. For this ideal case, a sensitive IR camera is required. In addition, the constitutive parameters of the IR detector screen are optimized to produce a large temperature rise in the detector material for a small amount of absorbed energy.

For the Focal Plane Array (FPA) used to make the IR thermograms presented in this paper, temperature differences as small as ΔT = 9 mK can be detected.

Care is, therefore, exercised in the selection of the screen material not to significantly perturb the electric or magnetic field by the presence of the lossy material. The screen is designed to absorb from 1% to 5% of the incident power and to produce a temperature change of less than a few degrees.

Electric and magnetic fields produced by continuous wave (CW) sources operated in the sinusoidal steady-state mode are easy to measure because of the large amount of energy contained in the wave. Transients produced by High-Power Microwave (HPM) pulsed sources, especial repetitively pulsed sources, can also be measured if the average energy content in the pulse is high enough to raise the temperature of the detector screen above the minimum temperature sensitivity of the IR camera. The thermal mass of the detector screen holds the absorbed energy long enough to capture the IR thermogram of the pulse.

IR Detector Screen

Referring to equation (1), the detector screen material is tailored to respond to only one component of the field, e.g. by optimizing the values of the electrical conductivity σ and the imaginary part ε'' of the permittivity of the screen material relative to the imaginary part μ'' of the permeability of the material, the detector screen can be made sensitive to either the tangential component of the electric field or the tangential component of the magnetic field in the plane of the screen.

For example, an *electric* field detector screen can be constructed either i) from a lossy material with high conductivity σ and low imaginary permittivity ε'' and low imaginary permeability μ'' or ii) from an electrically polarizable material with high imaginary permittivity ε'' and low conductivity σ and low imaginary permeability μ''.

Alternatively, a *magnetic* field detector screen can be constructed from a magnetically polarizable (magnetizable) material with high imaginary permeability μ'' and low conductivity σ and low imaginary permittivity ε''.

The optimization of the thermal and electrical parameters of the detection screen material is guided by an electromagnetic/thermal (EMT) computer code based on a plane wave obliquely incident on a planar interface between air and the lossy detector screen material. Other absorptive and re-emittive transducing materials [7-9] have been studied for use as passive thermal screens for infrared scene discrimination. In the examples that follow, only the electric field detector is considered in this article.

Electric Field Detector Screen. For the detection of electric fields, the IR detection screen can be made from a thin, planar sheet of carbon paper (e.g., Teledeltos Paper) or a carbon loaded polyimide film (e.g., Kapton). The detector screen used to make the electric field thermograms presented in this article has a conductivity of 8 mhos/meter and is 80 μm thick. This material is non-polarizable and non-conducting; therefore, the imaginary components of the permittivity ε'' and the permeability μ'' are negligibly small. For this conducting, non-polarizable, non-magnetic detector screen material, maximum heating occurs due to the electric field and negligible heating occurs due to the magnetic field.

For plane waves normally incident on this carbon loaded electric field detection screen and for an IR FPA with a temperature sensitivity as small as 9 mK, electric fields with a magnitude on the order of 61.4 V/m (1 mW/cm^2 of incident power) can be easily detected. This result was obtained empirically from experimental data in which the incident power level was incrementally decreased until no electric field contours were discernable on the IR thermogram from the ambient background level.

IR Camera

The temperature difference between the detector screen material and the background is detected, digitized, and stored in the memory of an IR camera on a pixel by pixel basis. The FPA system used for this article has 256 by 256 pixels per frame of data. Each pixel is an Indium Antimonide (InSb) IR photo detector operated in a photo-voltaic mode. The array operates at liquid Nitrogen temperatures and is enclosed in a dewar.

IR Images

The stored thermal data represents the temperature distribution over the extent of the detector screen and is a map (image) of the intensity of the electric or magnetic field distribution absorbed in the screen. For small temperature rises less that a few degrees, the electric and magnetic field intensities are nearly linearly proportional to the temperature change.

Spatial Resolution. The spatial resolution of the IR thermogram is a function of the number of pixel elements in the FPA and is fixed by the angular resolution of the wide angle, normal, or telephoto lens used on the IR camera when taking the IR image. The telephoto lens can be used to look at small details of the field structure on the detector screen; the wide angle lens can be used to look at large scale trends in the field structure on the detector screen.

The telephoto lens also has the added advantage for regular field mapping applications of allowing the IR camera to be located a long distance away from the object under test, and, thus, removing any perturbing effects that the metallic structure of the camera might have on the field distribution being measured.

Thermal Resolution. The thermal resolution of the IR thermogram is a function of the digitizer in the FPA. The FPA used to take the IR thermograms presented in this article uses a 12 bit digitizer. For a 12 bit digitizer, the temperature range seen by the IR camera is divided into 256 increments. Each digitized increment is assigned a unique color, resulting in a temperature resolution of 256 color levels.

Thermal Errors. The resulting IR image of an EM field depends on the combined EM and thermal properties of the detector material and is subject to several small and controllable errors.

***Lateral Conduction Effects*.** Conductive heating in the transverse direction within the screen material causes thermal "blurring" from the hot spots on the screen to nearby cold spots. This thermal blurring tends to fill in the nulls (minimums) somewhat, whereas, the areas of maximum heating (peaks) are not effected very much by this effect. This effect can be minimized by operating at small temperature variations above ambient.

Lateral Convective Effects. Convective heating of the top of the screen due to heat rising from the bottom of the screen causes the top of the screen to appear slightly hotter than the bottom of the screen. This thermal "bleeding" of the image can be kept to a minimum by operating at small temperature variations above ambient. This bleeding effect can be eliminated completely by placing the IR detector screen in a horizontal position and observing the image with the IR camera looking down on the screen from above or from the side using an IR mirror.

IR Measurement Accuracy

The accuracy of the IR measurement technique can be demonstrated by performing a simple experiment with a known theoretical solution. In this experiment, as shown in *figure 1,* the diffraction pattern from "Lloyd's Mirror" was measured.

In the Lloyd's mirror experiment, the resulting diffraction pattern is caused by the antenna interfering with its image in a large ground plane. The second peak in *figure 1* is smaller in magnitude than the first peak because the radiation pattern of the horn antenna used in the experiment decreases with angle from the bore sight direction of the horn. The near-field (Fresnel Zone) antenna pattern of the horn antenna was used to obtain the theoretical results.

The screen material was optimized to measure only the tangential component of the electric field intensity in the plane of the screen.

This experiment was performed in an anechoic chamber, as shown in *figure 1a*. Good correlations between theory and experiment were obtained, as shown in *figure 1b*. The worst errors occurred in the minimums (deep nulls) of the diffraction patterns were thermal blurring from the surrounding hot areas tended to obscure the real depth of the minimums. Some thermal blurring out of the maximums into the surrounding areas also occurred, obscuring the real height of the maximums.

Even with conductive blurring and convective bleeding of the image, the measurement error is less than approximately 10% under normal controlled test conditions.

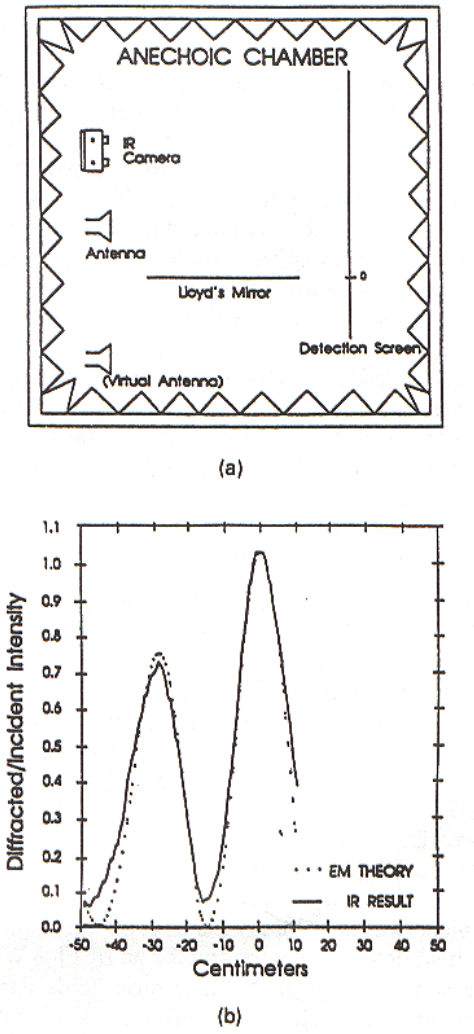

Figure 1. "Lloyd's Mirror" experiment (an antenna near a large ground plane) – correlation between theory and experiment: (a) IR experimental setup (looking down into the anechoic chamber) and (b) near-field diffraction pattern from a finite ground plane (along a horizontal line through the center of the IR detection screen).

IR Advantages and Disadvantages

The IR measurement technique provides a quick and accurate method to observe EM fields in a two-dimensional plane. However, only the magnitude of the electric or magnetic field is measured; no phase information is detected. Also, since this technique is based on the thermal mass of a detector material, high energy is required to produce good thermal images of EM fields.

IR THERMOGRAMS

Some examples of measured IR thermograms of electric fields are presented below.

IR Thermograms of Electric Fields

Radiation from a Horn Antenna, and Scattering from and Coupling into a Cylinder

As an example of the IR measurement of electric fields, a right circular cylinder, containing a long, thin slot aperture in its side, was irradiated with a plane EM wave from a pyramidal horn antenna. IR thermograms were made of the radiation pattern of the horn, the diffraction pattern of the EM field scattered from the cylinder, and the cylindrical modes excited inside the cavity. The experimental setup is shown in *figure 2*.

Aperture Coupling into a Finite Cylinder. The experimental cylinder is one meter in length and has an inner diameter of approximately 10 centimeters. The rectangular slot aperture is 64 millimeters in width and is 10 centimeters in length. The slot is located in the middle of the cylinder and is oriented parallel to the axis of the cylinder. The cylinder is irradiated with microwave energy at 3 GHz (10 centimeter wavelength) from a pyramidal horn antenna, polarized in the circumferential direction of the cylinder. Cylindrical TE modes are predominantly excited by the wave polarization inside the cavity.

A large IR detector screen of carbon paper was positioned in the transverse radial plane that intersected the middle of the slot aperture. Another IR disk was positioned inside the cylinder in the same cross-sectional plane.

Experimentally obtained IR thermograms of the results are shown in *figures 3 through 5*. The brightness of each color in the image corresponds to the intensity of the EM field. The radiation pattern of the horn, the diffraction patterns of the EM fields scattered from the cylinder, and the modal patterns of the induced cylindrical cavity modes are clearly indicated in these figures.

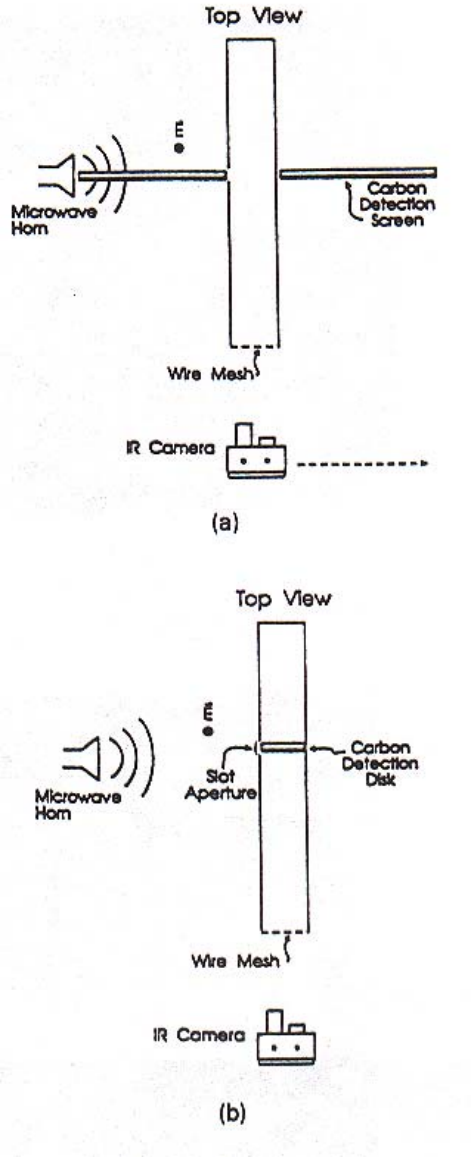

Figure 2. Experimental arrangement for IR images of plane wave scattering from a finite-length cylinder and slot aperture coupling into a cylindrical waveguide cavity. (a) IR camera and detector screen setup for measuring exterior scattered fields. (The IR camera is positioned on either side of the cylinder.) (b) IR camera and detector screen for measuring interior cylindrical waveguide cavity modes. (The IR camera is positioned on the axis of the cylinder and looks through a wire mesh screen simulating a microwave shield – microwave opaque, optically transparent).

Thermograms of the incident microwave field of the pyramidal horn antenna are shown in *figure 3*. *Figure 3(a)* is an image of the electric field traveling wave in the longitudinal plane in front of the horn. *Figure 3(b)* is an image of the electric field in the transverse near-field plane one meter in front of the aperture of the horn. Thermograms of the field scattered from the cylinder are shown in *figure 4*. *Figure 4(a)* is the image of the electric field standing wave created between the horn and the cylinder. This thermogram shows the interference pattern between the incident wave and the scattered cylindrical wave. *Figure 4(b)* is an image of the electric field traveling wave in the shadow zone of the cylinder. The null behind the cylinder and the diffracted wave off the top and bottom of the cylinder can be seen in this thermogram. Thermograms of the induced modes coupled into the cylindrical cavity are shown in *figure 5*. *Figure 5(a)* is an image of the electric field coupled through the aperture for a frequency 10% below the cutoff frequency of the cylindrical waveguide. The EM energy coupled through the aperture is visible in this thermogram and, as expected, has the radiation pattern of an electric dipole. The dominant TE_{11} waveguide modal pattern is partially developed in the center of the waveguide. *Figure 5(b)* is an image of the electric field coupled through the aperture for a frequency 10% above the cutoff frequency of the cylindrical waveguide. The dominant TE_{11} waveguide modal pattern is now fully developed in the center of the waveguide.

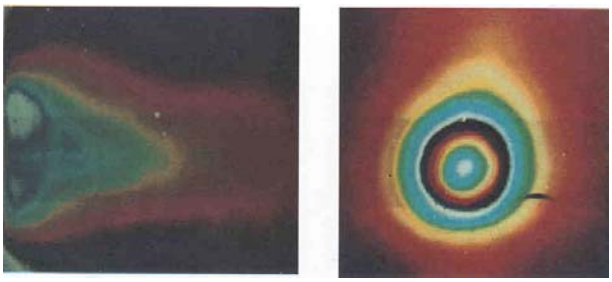

(a) (b)

Figure 3. IR thermograms of a microwave horn radiation pattern (a) in the longitudinal plane (in the vertical plane through the center of the horn aperture and (b) in the transverse plane (a cross-sectional cut of the microwave beam 1m in the near field in front of the aperture plane).

(a) (b)

Figure 4. IR thermograms of the diffraction pattern of the scattered electric field from a finite cylinder: (a) standing wave between the horn and the cylinder (showing the constructive and destructive interference patterns between the incident and reflected waves) and (b) traveling wave behind the cylinder (showing the shadow zone behind the cylinder and the surface diffracted waves).

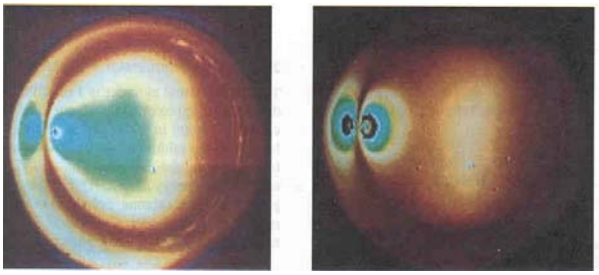

(a) (b)

Figure 5. IR thermograms of the excited cylindrical waveguide cavity mode inside the cylinder (the long, thin horizontal slot aperture is located in the center of the left-hand side of the IR thermograms - note the reflection in the walls of the waveguide – parallax effect): (a) excitation of an evanescent mode (at a frequency 10% below cutoff) and (b) excitation of the dominant TE_{11} cylindrical waveguide mode (at a frequency 10% above cutoff - note the dipole pattern at the aperture, as predicted by Bethe hole coupling theory).

In the above thermograms, note that the IR camera used to take the thermograms was one of the early models of a FPA Staring array and the IR detector screen was made from a Kapton film. The thermograms shown are the original raw data directly off the camera. The white spots are bad pixels, which were easily removed using a simple nearest neighbor averaging scheme. In addition, for an easy test setup, the thermograms were taken with a vertical detector screen. The distortion of the image (which should be symmetrical - top to bottom) caused by thermal bleeding of the extra heat from the bottom to the top of the picture is clearly seen in thermogram 3(b). This is eliminated when using a horizontal screen. Finally, note that the black horizontal mark to the lower right of center in thermogram 3(b) is a mechanical flaw (non-uniformity in surface conductivity) in the Kapton film, which was later processed out of the digital image.

CEM Code Validation

A scale model of a F16 aircraft was made. A 1/64th plastic scale model was spray-painted with several coats of silver paint to make it conductive. The scale model was cut into the carbon screen so that the wings of the airplane were in the plane of the paper. This scale model was illuminated by a horn antenna at different frequencies, angles of incidence, and polarizations. The screen was also moved into a transverse plane through the middle of the wings of the aircraft and the process repeated. The experiment was performed inside the anechoic chamber at the Air Force Research Laboratory at the Phillips Research Site (AFRL/PRS). The test setup is shown in figure 5 for the test case of normal incidence with the screen in the plane of the wings. The resulting IR thermogram is shown in Figure 6. Note the standing wave setup in front of the aircraft between the incident spherical wave from the horn antenna and the reflected wave from the nose of the aircraft. The transparent radome is not included in the model of the aircraft; however, the radome, which houses the Fire Control Radar (FCR), is included in the model. A surface wave has also developed on both sides of the aircraft between the nose of the aircraft and the missile rails on the wing tips. Diffraction off the trailing edge of the wingtips is evident in the thermogram, as is the shadow zone behind the aircraft.

A similar numerical study of the F16 was done at the Air Force Research Laboratory at the Rome Research Site (AFRL/RRS) using the *General Electromagnetic Model for the Analysis of Complex Systems* (*GEMACS*) code on a full size F16 aircraft. The code was run on a CRAY computer at Los Alamos National Laboratory (LANL). The numerical results were compared to experiments performed on the aircraft at the "upside down" Air Force facility at the Newport test site.

The results from the numerical code are presented in Figures 7 and 8. Figure 7 is a map of the surface currents on the aircraft; figure 8 is a picture of the scattered fields. The experimental results from the IR

measurements compare well to the numerical results from the *GEMACS* code. Note that the (*GEMACS*) code was run with a plane wave incident on the aircraft, whereas, in the measurements, the source produced a spherical wave in the far field at the location of the model.

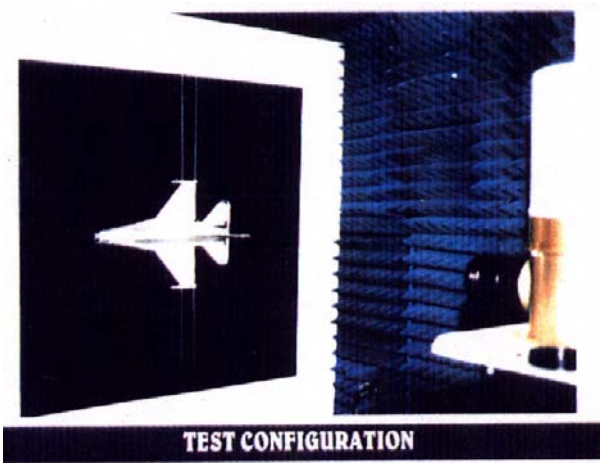

Figure 5. Test setup for scale model F16. Normal incidence in the plane of the wings.

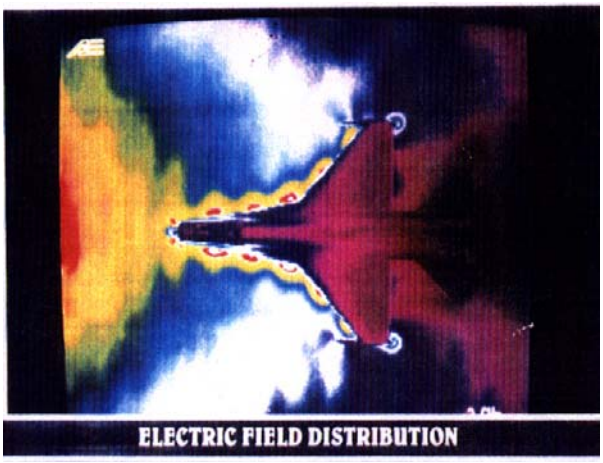

Figure 6. Test results for scale model F16. IR thermogram for normal incidence in the plane of the wings.

CONCLUSION

The IR measurement technique is a viable method to aid in the determination of EM fields radiated from antennas, scattered from complex metallic objects, and coupled into complex cavity structures. This method is of particular importance in the study of scattering objects with complicated geometrical shapes, whose field patterns may not be found easily using theoretical methods.

The IR method allows for rapid observation of EM field activity and interference, resulting in an in-depth understanding of the EM radiation, scattering, and coupling phenomena. Qualitative and quantitative comparisons can be made between the fields measured using the thermal radiation experimental approach and the fields predicted using a theoretical/numerical approach. Experimental and theoretical data, therefore, can be easily correlated with this technique.

Test results similar to those reported here have been used in the past to validate other numerical codes [10,11].

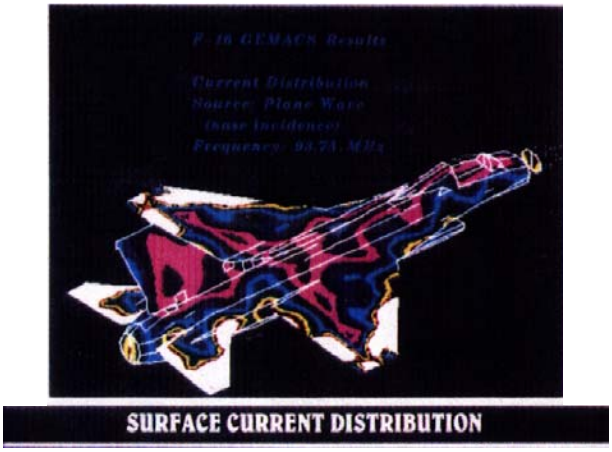

Figure 7. F16 surface currents from the *GEMACS* code.

Figure 8. F16 scattered fields from the *GEMACS* code.

ACKNOWLEDGEMENT

The author would like to acknowledge the help and support of this IR project from his colleagues Carl Stubenrauch at NIST/Boulder, Mike Harrison, Bill Prather, Hugh Pohle, and Joe Sadler at the Microwave Research Laboratory at the USAF Phillips Laboratory and Jerry Genello and Steve Lapree at the EM Vulnerability Laboratory USAF Rome Laboratory.

REFERENCES

[1] D.W. Metzger, J.D. Norgard and R.M. Sega, "Near-Fields Patterns from Pyramidal Horn Antennas: Numerical Calculation & Experimental Verification" *IEEE-EMC Transactions*, Vol. 33, No. 3, August 1991, pp. 188-196.

[2] R.M. Sega and J.D. Norgard, "Infrared Measurement of Scattering and Electromagnetic Penetrations through Apertures," *IEEE-NS Transactions*, Vol. NS-33, No.6, December 1986, pp. 1858-1883.

[3] J.D. Norgard, R.M. Sega, K.J. Ianacone, M.G. Harrison, A.T. Pesta and M.A. Seifert, "Scattering Effects of Electric and Magnetic Field Probes," *IEEE-NS Transactions*, Vol. NS-36, No. 6, December 1989, pp. 2050-2057.

[4] R.M. Sega and J.D. Norgard, "An Infrared Measurement Technique for the Assessment of Electromagnetic Coupling," *IEEE-NS Transactions*, Vol. 32, No. 6, December 1985, pp. 4330-4332.

[5] R.M. Sega, J.D. Norgard and G.J. Genello, "Measured Internal Coupled Electromagnetic Fields Related to Cavity and Aperture Resonance," *IEEE-NS Transactions*, Vol. NS-34, No. 6, December 1987, pp. 1502-1507.

[6] J.D. Norgard, D.C Fromme and R.M. Sega, "Correlation of Infrared Measurement Results of Coupled Fields in Long Cylinders with a Dual Series Solution," *IEEE-NS Transactions*, Vol. NS-37, No. 6, December 1990, pp. 2138-2143.

[7] W.H. Purdy and W.E. Woehl, "A Passive Thermal Screen for Infrared Scene Simulation," *Optical Engineering,* Vol. OE-15, No. 6, December 1976, pp. 554-558.

[8] V.T. Bly, "Passive Visible to Infrared Transducer for Dynamic Infrared Images Simulation," *Optical Engineering,* Vol. OE-21, No. 6, December 1982, pp. 1079-1082.

[9] M.J. Scholl, "Thermal Considerations in the Design of a Dynamic IR Target," *Applied Optics*, Vol. 21, No. 4, February 1982, pp. 660-667.

[10] R.W. Ziolkowiski and J.B. Grant, "Scattering from Cavity Backed Apertures: The Generalized Dual Series Solution of the Concentrically Loaded E-Pol Slit Cylinder Problem," *IEEE-APS Transactions*, Vol. AP-13, No. 5, May 1987, pp. 504-528.

[11] R.W. Ziolkowiski, W.A. Johnson and K.F. Casey, "Applications of Reimann-Hilbert Problem Techniques to Electromagnetic Coupling through Apertures," *Radio Science*, Vol. 19, No. 6, November-December 1984, pp. 1425-1431.